Multi-phase-field approach to fracture demonstrating the role of solid-solid interface energy on crack propagation

Hossein Jafarzadeh · Oleg Shchyglo ·
Ingo Steinbach

Abstract A multi-phase-field approach for crack propagation considering the contribution of the interface energy is presented. The interface energy is either the grain boundary energy or the energy between a pair of solid phases and is directly incorporated into to the Ginzburg–Landau equation for fracture. The finite difference method is utilized to solve the crack phase-field evolution equation and fast Fourier method is used to solve the mechanical equilibrium equation in three dimensions for a polycrystalline material. The importance of the interface (grain boundary) energy is analyzed numerically for various model problems. The results show how the interface energy variations change the crack trajectory between the intergranular and transgranular fracture.

H. Jafarzadeh (✉)
Department of Mechanical Engineering, Isfahan University of Technology, Isfahan 84156-83111, Iran
e-mail: jafarzadeh@iut.ac.ir;
hossein.jafarzadeh@ruhr-uni-bochum.de

H. Jafarzadeh · O. Shchyglo · I. Steinbach
Interdisciplinary Center for Advanced Material Simulations, Ruhr-Universität Bochum, Universitätsstr. 150, 44801 Bochum, Germany

1 Introduction

Interface energy plays an important role in materials science and many engineering applications, such as adhesion (Yin etal. 2022), void dynamics (Ghaedi and Javanbakht 2021), wetting (Jafarzadeh et al. 2019), phase transformations (Levitas and Javanbakht 2011), and fracture (Jafarzadeh et al. 2019). The interface energy can be controlled for designing materials with specific properties and improving the performance of devices that rely on interfaces, such as electronic devices, solar cells, and batteries. Understanding the mechanisms and characteristics of interfacial fracture is crucial for designing materials and structures with improved resistance to failure, as well as for developing strategies to tailor interfacial properties for specific applications.

The phase-field method provides a powerful computational tool to study a range of complex phenomena, such as plasticity (Levitas and Javanbakht 2012), twinning (Clayton and Knapp 2011, Amirian et al. 2022a, Amirian et al. 2022b), martensitic phase transformations (Levitas and Preston 2002, Rahbar et al. 2022, Shchyglo et al. 2019), damage (Fantoni et al. 2020), fatigue (Mesgarnejad et al. 2019; Grossman-Ponemon et al. 2022), and fracture (Msekh et al. 2016; Amiri et al. 2016; Karma et al. 2001, Hofacker and Miehe 2012, Clayton and Knap 2014, Farrahi et al. 2020, Jafarzadeh and Mansoori 2020). Within the multi-phase-field approach for fracture, the crack surfaces and the solid-solid interfaces each are represented by

the continuous fields named "order parameter" as a diffuse boundary with finite thickness, rather than a sharp and discontinuous surface/interface. The order parameter in phase-field models have different interpretations. In the context of fracture, cracks represent narrow regions with a strong variation of the associated order parameter. Then the phase-field approach is used to capture crack nucleation, propagation, branching, and coalescence in a wide range of materials and structures more efficiently than using sharp interface methods. The problem of interface energy and interface stresses has been addressed in different phenomena using the phase-field approach (Ghaedi and Javanbakht 2021, Jafarzadeh et al. 2019, Levitas and Javanbakht 2011). Recently, the surface stresses were incorporated into fracture both at small (Levitas et al. 2018, Jafarzadeh et al. 2020) and large strains (Jafarzadeh et al. 2022). However, the number of publications considering the effect of interface energy within the phase-field approach to fracture is scarce.

Spatschek et al. 2007 presented a continuum theory for elastically induced phase transitions to describe fracture by using double-well potential. They also generalized their model to multi-phase simulations. Note that a comprehensive comparison between single-well potentials and double-well potentials is presented in Levitas et al. 2018. A phase-field model for fracture in ferroelectric polycrystals was presented by Abdollahi and Arias 2012. They interpolated the critical energy release rate in a polycrystal between a maximum value for the inside of the grains and its minimum indicating the ratio of the critical fracture energy of the grain boundary to that of the grain interior. By changing this ratio, they studied the transition between the intergranular and transgranular modes of crack growth. They used single-well potential for crack in the spirit of Francfort and Marigo (1998). Oshima et al. (2014) constructed a multi-phase-field crack model allowing to simulate crack propagation in Polycrystalline materials. They used the multi-phase-field model proposed by Steinbach and Pezzolla 1999 and utilized the double-well potential. Hossain et al. 2014 proposed a definition for the effective toughness of a heterogeneous media that is a material property, independent of the details of the boundary condition. They also proposed a numerical approach to compute the effective toughness. Phase-field modeling of crack propagation in multi-phase systems based on Griffith's theory was presented by Schneider et al. 2016. They combined the single-

obstacle potential for fracture with a multi-obstacle potential for multiple grains adopted from Nestler et al. 2005. The comparison between single-obstacle potential and single-well potential for fracture is made in Schneider et al. (2016) and more general and more comprehensive in Jafarzadeh et al. 2022. They concluded that reaching the grain boundary region, the crack tip velocity rises because the interfacial energy degrades additionally Schneider et al. 2016. The same conclusion has been made when crack reached the austenite-martensite interface (Jafarzadeh et al. 2019). Hansen Dörr et al. 2019 proposed a phase-field approach for failure of the interface between two possibly dissimilar materials where the fracture toughness of an adhesive interface is smaller than that in the bulk of the material. While all previous models use a single-crack order parameter, a phase-field model with multiple crack order parameters was introduced by Schöller et al. 2022. Each of the crack order parameters only tracks the damage in the corresponding phase. This results in multiple evolution equations, each of which has a constant crack surface energy. They showed the applicability of the model to a 3D system. However, all other studies mentioned above had been conducted in 2D.

Here we propose a new approach based on considering the interface energy dependent on the fracture parameter. In the most general case, one can assume that the interface energy vanishes when crack goes through the interface. Jafarzadeh et al. 2019 used this approach to study coupled fracture and martensitic behaviors. We take the multi-solid-phase potential from Steinbach 2009 and crack potential from Jafarzadeh et al. 2022. The current crack potential has the advantages of both single-obstacle potential and single-well potential.

In the following, vectors and tensors are designated with boldface symbols. Contractions of tensors $A = A_{ij}$ and $B = B_{ij}$ over one and two indices are $A \cdot B = \{A_{ij} B_{jk}\}$ and $A : B = A_{ij} B_{jk}$, respectively. ∇ stands for the gradient operator.

2 Phase-field approach to fracture in one-phase material

For the crack order parameter, we introduce ϕ_c (subscript c stands for crack) and include it later as an internal variable in the free energy functional. ϕ_c characterizes bond weakening in a solid and continuously describes the sample into the following three regions:

intact solid ($\phi_c = 0$), completely broken bonds ($\phi_c = 1$), and a finite width in which the material is partially broken ($0 < \phi_c < 1$). In all these regions the continuity in displacement field is ensured as a feature of phase-field approach. The evolution of the damage order parameter occurs mainly in the crack tip zone. Thus, the damage growth is characterized by the evolution of the crack phase-field determined by the Ginzburg-Landau equation.

The free energy density formulation follows the well-established phase-field approach to fracture (Levitas et al. 2018, Jafarzadeh et al. 2022):

$$\psi = I(\phi_c)\Psi^e(\boldsymbol{\varepsilon}) + Af(\phi_c) + \frac{\beta}{2} \mid \boldsymbol{\nabla}\phi_c \mid^2, \qquad (1)$$

where the first term is the elastic free energy as a function of the strain tensor $\boldsymbol{\varepsilon}$. The second and the third terms produce fracture energy which are the cohesion and gradient contributions, respectively. Ψ^e is the elastic energy of damage-free strained material. $I(\phi_c) = (1 - \phi_c)^2$ is the monotonously decreasing degradation function from 1 at intact phase ($\phi_c = 0$) to 0 at the broken phase ($\phi_c = 1$), which is well-accepted in the literature (Francfort and Marigo 1998, Levitas et al. 2018, Jafarzadeh et al. 2022). $f(\phi_c)$ is the interpolation function which is adopted from Jafarzadeh et al. 2022 in the form of $f(\phi_c) = \frac{k\phi_c^2+\phi_c}{k+1}$. However we choose $k = 1$ as

$$f(\phi_c) = \frac{\phi_c^2 + \phi_c}{2}, \qquad (2)$$

which satisfies the mandatory conditions $f(0) = 0$ at $\phi_c = 0$ and $f(1) = 1$ at $\phi_c = 0$. This potential allows for finite region of the damaged zone in contrast to the single-well potential $f(\phi_c) = \phi_c^2$ as a special case of $f(\phi_c) = \frac{k\phi_c^2+\phi_c}{k+1}$ in the limit of infinite k. This will be shown in Eq. 9 below. In addition, it produces more physical equilibrium stress–strain curve than single-obstacle potential $f(\phi_c) = \phi_c$ as a special case of $f(\phi_c) = \frac{k\phi_c^2+\phi_c}{k+1}$ where $k = 0$. The complete analysis can be found in Jafarzadeh et al. 2022. A and $\beta \geq 0$ are the maximum cohesion energy for the completely-damaged state and the gradient coefficient, respectively. Both will be determined below.

The Ginzburg–Landau evolution equation which describes crack nucleation and propagation reads

$$\dot{\phi}_c = -L\delta\psi/\delta\phi_c = -L\left(\frac{\partial\psi}{\partial\phi_c} - \boldsymbol{\nabla}\cdot\left(\frac{\partial\psi}{\partial\boldsymbol{\nabla}\phi_c}\right)\right)$$
$$= -L\left(\frac{\partial\psi}{\partial\phi_c} - \beta\boldsymbol{\nabla}^2\phi_c\right), \qquad (3)$$

where L is the kinetic coefficient and we used the functional derivative $\delta\psi/\delta\phi_c$.

The calculation of the elastic energy from unloaded state to completely damaged state gives us the maximum cohesion energy, A (Levitas et al. 2018):

$$\int_0^{\boldsymbol{\varepsilon}_c} \boldsymbol{\sigma} : d\boldsymbol{\varepsilon} = A, \qquad (4)$$

where $\boldsymbol{\sigma} = \frac{\partial\psi}{\partial\boldsymbol{\varepsilon}}$ is the stress tensor and $\boldsymbol{\varepsilon}_c$ is the strain at $\phi_c = 1$. For uniaxial tension, stress work is equal to the area under the stress–strain curve (Levitas et al. 2018).

The elastic stress work within the volume $S(2d)$ corresponding to two diffuse crack volumes, where d is defined as surface width length scale, is equal to the crack resistance energy G which is defined per unit area. Thus, $A(2Sd) = GS$ and we obtain

$$A = \frac{G}{2d}. \qquad (5)$$

The fracture energy resulting from creation of two surfaces is the non-mechanical energy excess with respect to the intact phase. On the other hand, the stationary solution of Ginzburg-Landau equation Eq. 3 results in $\psi^c = \psi^\nabla$, which means that the excess of the local energy is equal to the gradient energy at equilibrium (Levitas et al. 2018). Then we can evaluate the fracture energy in 1D as follows

$$G = \int_{-\infty}^{\infty} (Af + \psi^\nabla)d\zeta = 2A\int_{-\infty}^{\infty} f d\zeta$$
$$= 4A\int_{-\infty}^{0} f d\zeta = 4A\int_0^1 f\frac{d\zeta}{d\phi}d\phi$$
$$= 2\sqrt{2A\beta}\int_0^1 \sqrt{f}d\phi = 2\sqrt{2A\beta}Y, \qquad (6)$$

where ζ is in the direction of normal to the diffuse planes and $Y := \int_0^1 \sqrt{f}d\phi$ is a number less than unity that can be evaluated, at least numerically, for any interpolation function $f(\phi_c)$. It follows from Eq. 6, allowing for Eq. 5 that:

$$\beta = \frac{G^2}{8AY^2} = \frac{Gd}{4Y^2}, \tag{7}$$

where for the current potential, Eq. 2, gives $\beta = 0.708Gd$.

Note that at nano scale the elastic stress work within the volume Sd should be equal to the created surface energy. Thus, $ASd = 2\gamma S$, where γ is the surface energy per unit area. In addition, $\int_{-\infty}^{\infty}(Af + \psi^{\nabla})d\xi = 2\gamma$ explains the difference between the nanoscale model (Levitas et al. 2018) where the fracture energy is described purely by surface energy ($A = \frac{2\gamma}{d}$ and $\beta = \frac{\gamma d}{4Y^2}$), and macroscale models where ($A = \frac{G}{2d}$ and $\beta = \frac{Gd}{4Y^2}$).

Finally, we obtain the free energy as:

$$\psi = (1 - \phi_c)^2 \frac{1}{2}\boldsymbol{\varepsilon} : \boldsymbol{C} : \boldsymbol{\varepsilon}$$
$$+ \frac{G}{2d}\left(\frac{\phi_c^2 + \phi_c}{2} + 0.708d^2 \mid \nabla\phi_c \mid^2\right), \tag{8}$$

where quadratic elastic energy is used and $\boldsymbol{C}$ is elastic moduli tensor of the intact state. Here, the elastic energy does not prevent fracture under compressive loads which is avoided in the following analysis. A new phase-field approach to fracture which treats the compressive loads as well is currently under development. The equivalence of the local energy and the gradient energy at free surfaces (the second and the third terms in Eq. 8) is analytically solved in 1D which gives the stationary distribution of $\phi_c = \phi_c(\zeta)$ in the form of

$$\begin{cases} \frac{\sqrt{\phi_c} + \sqrt{\phi_c + 1}}{1 + \sqrt{2}} = e^{-0.42\frac{|\zeta|}{d}} & \text{if } \zeta < \zeta_t; \\ 0 & \text{if } \zeta > \zeta_t, \end{cases} \tag{9}$$

where $\phi_c = 1$ corresponds to the separation plane at $\zeta = 0$ and $\zeta_t = 1.65d$ is the transition plane from the damaged state to the intact state. More detailed derivation of Eq. 9 can be found in Jafarzadeh et al. 2022.

3 Multi-phase-field approach for for solid-solid phase transformation

Multi-phase-field approach is used to deal with an arbitrary number of different phases or grains of the same phase, but distinct by their orientation. In this section, we do not consider solid-solid phase transformation, thus the evolution equations for ϕ_α is not used. Therefore, all we need from the multi-phase-field model is the interface energy contribution and interface profile which are taken from Steinbach's model (Steinbach 2009). Figure 1 shows the sharp and diffuse description of the interfaces and a triple junction in a three-phase system.

A set of order parameters ϕ_α is employed to describe different phases/grains in a multi-phase/polycrystalline material. The $\alpha = 1, \ldots, N$ subscripts stand for N number of solid phases. This set of the order parameters is used to distinguish each grain/phase from others either by its orientation or phase designation or both. ϕ_α continuously changes in the range from 0 to 1. $\phi_\alpha = 1$ in the pure phase α, $0 < \phi_\alpha < 1$ at the interface between phase α and other phase(s), and $\phi_\alpha = 0$ elsewhere.

The interface free energy per unit volume is given by

$$\psi^{int} = \sum_{\alpha=1}^{N-1}\sum_{\beta=\alpha+1}^{N}\frac{4\sigma_{\alpha\beta}}{\eta_{\alpha\beta}}\left[\phi_\alpha\phi_\beta - \frac{\eta_{\alpha\beta}^2}{\pi^2}\nabla\phi_\alpha\nabla\phi_\beta\right], \tag{10}$$

$$\sum_{\alpha=1}^{N}\phi_\alpha = 1, \tag{11}$$

where $\sigma_{\alpha\beta}$ and $\eta_{\alpha\beta}$ are the interface energy and interface width corresponding to each pair of different phases.

In a 1D case the interface energy for dual phase-field interface ψ_{1D}^{int} ($N = 2$, $\phi := \phi_2 = 1 - \phi_1$, $\nabla\phi_2 = -\nabla\phi_1$, $\eta := \eta_{12}$, and $\sigma := \sigma_{12}$) reduces to

$$\psi_{1D}^{int} = 4\sigma\left[\frac{1}{\eta}\phi(1 - \phi) + \frac{\eta}{\pi^2}\left(\frac{\partial\phi}{\partial\xi}\right)^2\right], \tag{12}$$

where ξ is in the direction of normal to the diffuse binary interface planes (Steinbach 2009). The equivalence of the local energy and the gradient energy (the first and the second terms in Eq. 12) at stationary interfaces gives the stationary distribution of $\phi = \phi(\xi)$ in the form of (Steinbach 2009)

$$\phi(\xi) = \frac{1}{2} - \frac{1}{2}sin\left(\frac{\pi}{\eta}\xi\right), \tag{13}$$

where $\phi(\xi) = 0$ and 1 correspond to the two different solid phases (grains) at $\xi = \frac{\eta}{2}$ and $-\frac{\eta}{2}$, respectively.

Fig. 1 Schematics of the **a** sharp and **b** diffuse interface in multi-phase-field approach

(a)   (b)
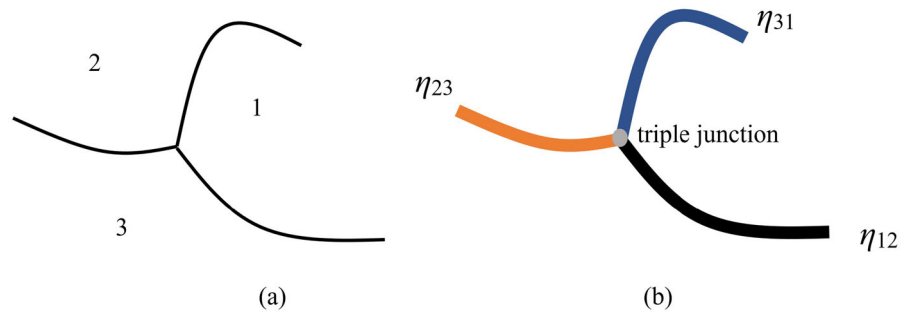
4 Phase-field approach to fracture in multi-phase material

4.1 *Order parameters*

The coupled description of fracture phase-field with description of the solid ↔ solid phase transformation by means of the sum convention upon all phase-field $\phi_c + \sum_{\alpha=1}^{N} \phi_\alpha = 1$ is presented in Schneider et al. 2016. This leads to Allen-Cahn equations for each single phase in the multi-phase system, including broken phase, with different mobilities. In their model, in the variation of the functional with respect to the crack phase-field ϕ_c, the interface energy of any arbitrary pair of solid phases $\sigma_{\alpha\beta}$ is not listed explicitly. However, the evolution equation for the order parameters is coupled with the dual interactions between all phases. Therefore, the interface energy is taken into account for the evolution of the crack phase-field, even if the mobility of the solid-solid interfaces vanishes.

The main feature of the current model is to decouple the description of solid ↔ solid phase transformation from the description of fracture. The kinetic and thermodynamic coupling of fracture with solid ↔ solid transformation is introduced in terms of energy description, as will be shown below. The fracture order parameter ϕ_c is equal to 0 in solid and 1 in broken phase. Solid phases are described by N order parameters ϕ_α such that $\phi_\alpha = 1$ in phase α and 0 in all other phases as discussed in the Sect. 3. For the solid ↔ solid phase transformations the sum constraint is imposed (Steinbach 2009)

$$\sum_{\alpha=1}^{N} \phi_\alpha = 1. \tag{14}$$

In Schneider et al. 2016 the fracture order parameter ϕ_c is presented geometrically along with all solid order parameters ϕ_α and is included in the summation rule $\phi_c + \sum_{\alpha=1}^{N} \phi_\alpha = 1$ as shown in Fig. 2a. In contrast, in our approach ϕ_c is described independent of ϕ_α as shown in Fig. 2b and does not belong to the solid order parameter plane. Figure 2b shows the geometrical description of Eq. 14 which is a plane in the order parameter space passing through all the solid phase order parameters. The ϕ_c-line (shown as a vector in Fig. 2b) starts from the solid plane where $\phi_c = 0$ and $\sum_{\alpha=1}^{N} \phi_\alpha = 1$, and ends at the origin which is the broken phase with $\phi_c = 1$ and still $\sum_{\alpha=1}^{N} \phi_\alpha = 1$. In this way we treat fracture as bond breaking rather than solid to crack phase transition or solid to gas phase transformation (Farrahi et al. 2020). Thus, diffuse crack surface is still a solid material with partially broken state. This allows us to capture surface induced phenomena (Jafarzadeh et al. 2019).

4.2 *Energy description*

We define the interface energy as the excess of the energy at the interface with respect to bulk, if the interface and bulk are in the same level of damage. The "if" is because of the surface energy contribution in the case of damage, as the damaged interface has higher energy than the intact interface. Based on this definition, we assume that in the equilibrium state, the excess of the energy in the interface decreases with increase in damage. Under such assumption $\sigma_{\alpha\beta}$ is replaced with $(1 - \phi_c)^2 \sigma_{\alpha\beta}$ as shown in Fig. 3. In the intact solid where $\phi_c = 0$ the interface energy is fully established and it degrades until the full damage happens where $\phi_c = 1$ and the interface energy becomes zero. With such assumptions, the effect of the interface energy on driving force of the crack propagation is already taken into account which is especially important when a crack propagates through the interface. Here we assume that

Fig. 2 Schematics of the order parameter space and the transformation paths. **a** Model used in Schneider et al. 2016, where fracture and all the transformation paths lie within the same plane. The figure is shown for two solid phases ($N = 2$) and one broken phase at the top corner. **b** Current model for which fracture path is decoupled from the transformation paths between solid phases. The figure is shown for three solid phases ($N = 3$) and one broken phase at the origin
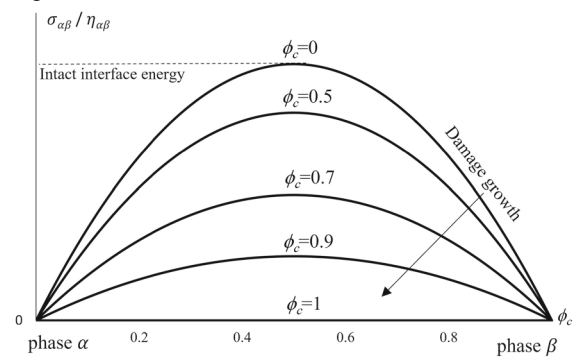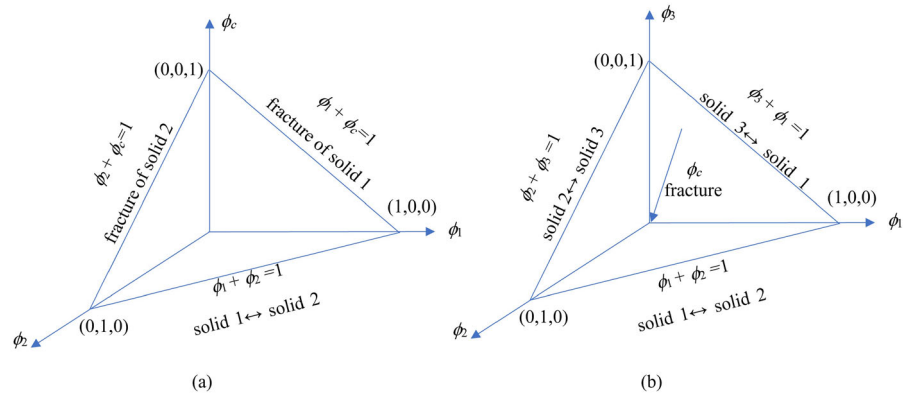

Fig. 3 Schematic of the interface energy for equilibrium interface. The area under each curve is equal to the degraded interface energy, $(1 - \phi_c)^2 \sigma_{\alpha\beta}$

the interface width does not depend on damage parameter i.e., it does not depend on how strong the atomic bonds are.

Taking into account the above assumptions, the general free energy description for fracture and solid $\leftrightarrow$ solid phase transformation reads

$$
\begin{aligned}
\psi = {} & (1 - \phi_c)^2 \frac{1}{2} \boldsymbol{\varepsilon} : \boldsymbol{C} : \boldsymbol{\varepsilon} \\
& + \frac{G}{2d} \left(\frac{\phi_c^2 + \phi_c}{2} + 0.708 d^2 \mid \nabla \phi_c \mid^2 \right) \\
& + (1 - \phi_c)^2 \sum_{\alpha=1}^{N-1} \sum_{\beta=\alpha+1}^{N} \\
& \times \left[\phi_\alpha \phi_\beta - \frac{\eta_{\alpha\beta}^2}{\pi^2} \nabla \phi_\alpha \nabla \phi_\beta \right],
\end{aligned}
\tag{15}
$$

$$
\sum_{\alpha=1}^{N} \phi_\alpha = 1, \tag{16}
$$

where all material properties are phase-dependent and interpolated for any intermediate state as follows

$$
\boldsymbol{C} = \sum_{\alpha=1}^{N} h^\alpha \boldsymbol{C}^\alpha, \tag{17}
$$

$$
G = \sum_{\alpha=1}^{N} h^\alpha G^\alpha, \tag{18}
$$

$$
d = \sum_{\alpha=1}^{N} h^\alpha d^\alpha. \tag{19}
$$

The interpolation function for the parameters has the following general form

$$
h^\alpha = \frac{g(\phi_\alpha)}{\sum_{\beta=1}^{N} g(\phi_\beta)}, \tag{20}
$$

which satisfies

$$
\sum_{\beta=1}^{N} h^\alpha = 1, \tag{21}
$$

and

$$
\frac{\partial h^\alpha}{\partial \phi_\alpha} = \frac{\dot{g}(\phi_\alpha)}{\sum_{\beta=1}^{N} g(\phi_\beta)}. \tag{22}
$$

$g(0) = 0$ and $g(1) = 1$ need to be satisfied as well. Thus, $g(\phi_\alpha)$ can be chosen as

$$
g(\phi_\alpha) = \phi_\alpha, \phi_\alpha^2, \phi_\alpha^2(3 - 2\alpha), ... \tag{23}
$$

In fact, $g(\phi_\alpha) = \phi_\alpha$ gives the relative fraction of the solid phase α and Eq. 15 reduces to Eq. 8 in the bulk (where without loss of generality $\phi_\alpha = 1$). In the

Ginzburg-landau equation for fracture, the interface energy of the solid phases $\sigma_{\alpha\beta}$ is explicitly included because it is degraded during fracture as shown in Eq. 15. This is in agreement with the model in Schneider et al. 2016 but treated differently. If the elastic moduli are constant and homogeneous, then the stress field is not affected by the grain boundaries, however by reaching the grain boundary region, the crack tip velocity rises because the interface energy $\sigma_{\alpha\beta}$ degrades additionally and consequently contributes to the driving force for crack growth. In a similar way this is shown for the case with martensitic phase transformation in Jafarzadeh et al. 2019.

One the other hand, the effect of different material parameters of different solid phases, such as fracture energy, on the deriving force for solid-solid phase transformation is taken into account. For example, it was shown that the difference between surface energies of martensite and austenite leads to wetting of the crack surface by martensite (Jafarzadeh et al. 2019).

Finally, we end up with only one evolution equation for fracture, Eq. 3, with the following free energy formulation

$$
\psi = (1 - \phi_c)^2 \frac{1}{2} \boldsymbol{\varepsilon} : \boldsymbol{C} : \boldsymbol{\varepsilon}
$$
$$
+ \frac{G}{2d} \left(\frac{\phi_c^2 + \phi_c}{2} + 0.708 d^2 \mid \nabla \phi_c \mid^2 \right)
$$
$$
+ (1 - \phi_c)^2 \sum_{\alpha=1}^{N-1} \sum_{\beta=\alpha+1}^{N} \frac{8 \sigma_{\alpha\beta}}{\eta_{\alpha\beta}} \phi_\alpha \phi_\beta; \qquad (24)
$$

where, for simplicity, the equivalence of the local potential term and gradient term is taken into account (Steinbach 2009, Farrahi et al. 2020). If the fracture is considered in polycrystalline material with equal grain boundary width η and grain boundary energy σ between any neighbor grains the Eq. 24 reduces to

$$
\psi = (1 - \phi_c)^2 \frac{1}{2} \boldsymbol{\varepsilon} : \boldsymbol{C} : \boldsymbol{\varepsilon}
$$
$$
+ \frac{G}{2d} \left(\frac{\phi_c^2 + \phi_c}{2} + 0.708 d^2 \mid \nabla \phi_c \mid^2 \right)
$$
$$
+ (1 - \phi_c)^2 \frac{8\sigma}{\eta} \phi(1 - \phi), \qquad (25)
$$

where the last term is 0 inside of the grains and has symmetric variation within the grain boundary. Similar procedure can be followed if one wants to use double-well potential for the interface energy which leads to

$$
\psi = (1 - \phi_c)^2 \frac{1}{2} \boldsymbol{\varepsilon} : \boldsymbol{C} : \boldsymbol{\varepsilon}
$$
$$
+ \frac{G}{2d} \left(\frac{\phi_c^2 + \phi_c}{2} + 0.708 d^2 \mid \nabla \phi_c \mid^2 \right)
$$
$$
+ (1 - \phi_c)^2 \frac{64\sigma}{\eta} \phi^2 (1 - \phi^2). \qquad (26)
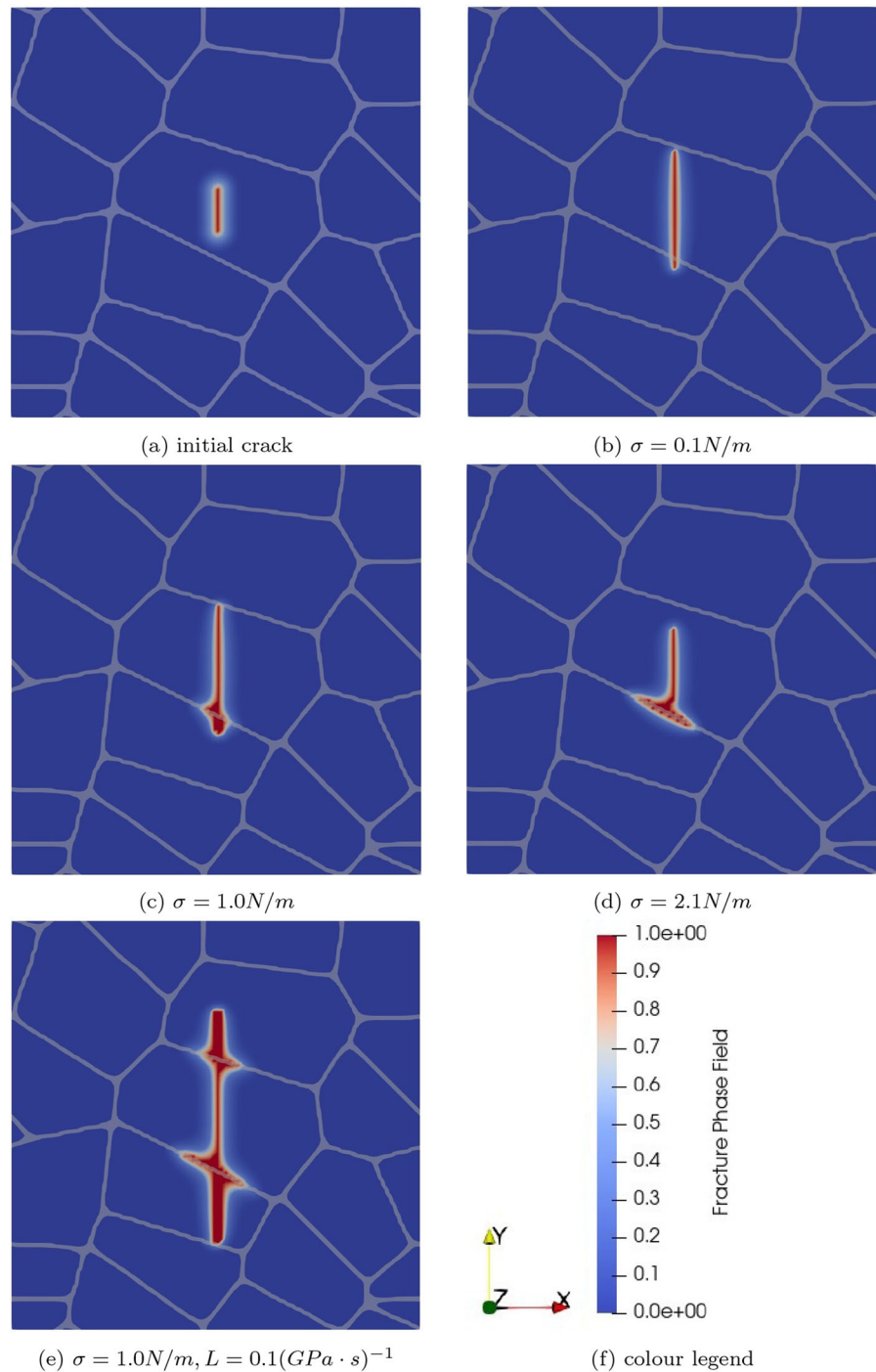$$

5 Results and discussions

5.1 Computational framework

The complete set of equations is implemented in Open-Phase [32] and solved to obtain the evolution of the crack and mechanical fields. The mechanical equilibrium problem is solved using the Khachatryan's elasticity model (Khachaturyan 1983) and the Fourier solver algorithm similar to Hu and Chen 2001. The periodic boundary conditions imposed by the Fourier space mechanical equilibrium solution require periodic simulation geometries. Therefore, periodic simulation geometries have been used in all simulations in this study. A 3.7 GHz (10 core) CPU was used to conduct the simulations. The 2D and 3D simulations lasted about 1 h and 1 day, respectively.

We highlight again that in the following examples the description of an actual grain growth is avoided and concentration is on the crack propagation. This is a well justified assumption because fracture and grain growth do not necessarily have the same order of kinetics. The coupled equations are: Ginzburg-Landau equation for crack in Eq. 3 along with the free energy in Eq. 15, kinematics $\boldsymbol{\varepsilon} = \frac{1}{2} (\nabla \boldsymbol{u} + \nabla \boldsymbol{u}^T)$, constitutive law $\boldsymbol{\sigma} = \boldsymbol{C} : \boldsymbol{\varepsilon}$, and equilibrium equations $\nabla \cdot \boldsymbol{\sigma} = \boldsymbol{0}$. $\boldsymbol{u}$ is displacement vector and superscript T stands for transpose operator. The grain structure is introduced by Voronoi tessellation in a periodic $100 nm \times 100 nm$ unit cell. The elastic moduli for the linear elastic material are taken as $C_{11} = C_{22} = C_{33} = 169 GPa$, $C_{12} = C_{13} = C_{23} = 138 GPa$ and $C_{44} = C_{55} = C_{66} = 15.5 GPa$. The kinetic coefficient is taken a very small value as $L = 0.05 (GPa \cdot s)^{-1}$ (Unless otherwise stated.) so that the crack growth is quasi-static. The strain of $\varepsilon = 0.023$ is applied at the lateral edges perpendicular to the initial crack line (in 2D examples) or crack surface (in 3D examples). To account for the interface energy cross effect with the surface energy we vary interface energy in different examples but keep the surface energy constant at $1 N/m$. Interface width and crack surface width

Fig. 4 Fracture phase-field for different grain boundary σ energy and kinetic coefficient L

(a) initial crack

(b) $\sigma = 0.1 N/m$

(c) $\sigma = 1.0 N/m$

(d) $\sigma = 2.1 N/m$

(e) $\sigma = 1.0 N/m, L = 0.1 (GPa \cdot s)^{-1}$

(f) colour legend

are $\eta = 3nm$ and $d = 6nm$. Equation 9 is used to introduce diffuse form of the initial crack surfaces at the middle of the simulation cells. Equation 13 is used to introduce a fully established interface in the initial state of a planar interface. However, for triple and higher junctions there is no analytical solution available. Then, the diffuse interface is established numerically by allowing the system reaching its equilibrium configuration by phase-field evolution.

5.2 2D example

In the first example we consider a straight crack line with a length of 10nm (see Fig. 4a and f for the colour legend). Figure 4b–d shows the crack shape at the end of the load for different values of the interface energy. In Fig. 4b the interface energy has negligible effect on the crack path. In this regime crack goes through the grains leading to transgranular fracture. In Fig. 4c, crack goes both through the grain and along the grain boundaries. In this regime, both transgranular and intergranular fracture are energetically comparable. However, in Fig. 4d, crack is mostly going through the grain boundaries rather than through the grains interior, which indicates purely intergranular fracture. These three cases show how the interface energy can affect the crack propagation direction and crack configuration. The higher interface energy material has the more deviation of the crack path from a straight line to the direction of the oblique grain boundary occurs. The effect of crack kinetics is shown in Fig. 4e where the damage zone is larger due to increased crack mobility compared to the example shown in Fig. 4c.

5.3 3D example

In order to emphasize the crack in 3D visualization, in this section the crack is shown by a red colour contour where $\phi_c < 0.9$ and the grain boundaries are shown in gray with reduced opacity. Figure 5 shows the grain structure with 15 different colours identifying 15 individual grains.

5.3.1 Centre-cracked plate

In this example a straight through-thickness crack surface with a length of 10nm (see Fig. 6a) is considered. Figures 6b–d show the crack shape at the end of the load for different values of the interface energy. In Fig. 4b where the interface energy is small, the crack is controlled by mechanical stresses and goes straight through the grains interior. In Fig. 4c,d crack trajectory is controlled both by elastic energy and interface energy, where higher interface energy leads to more broken grain boundaries. The fracture regime changes from transgranular fracture for low grain boundary energy (interface energy) to intergranular fracture for high grain boundary energy. The effect of crack kinetics
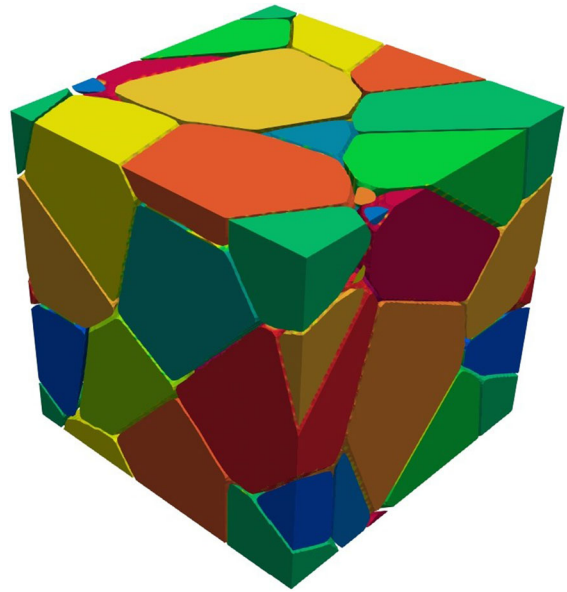

Fig. 5 Grain structure for fracture simulations

is illustrated by comparing Fig. 4c and Fig. 4e. Similar to the 2D case the higher crack mobility leads to larger damage zone.
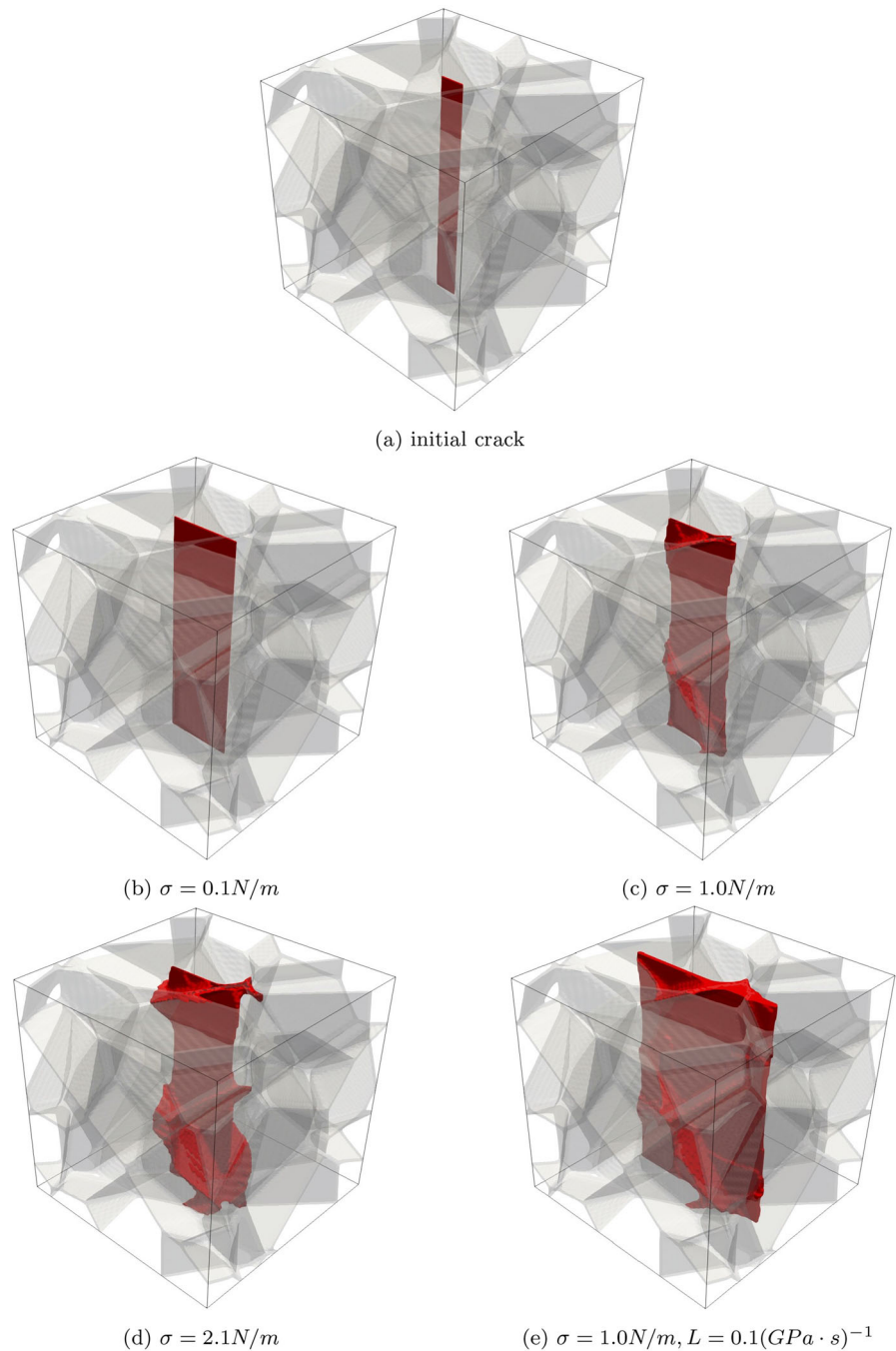
5.3.2 Penny-shaped crack

In this example a fully embedded circular crack with the radius of 10nm is introduced as shown in Fig. 7a. Figures 7b–d show the crack shape at the end of the load for different values of the interface energy. Figure 7b shows that the mechanical load is not sufficient for the crack to evolve even though there is a little interfacial driving force $\sigma = 0.1N/m$ for fracture. Figure 7c shows the importance of interface energy in fracture: the crack does not evolve with $\sigma = 0.1N/m$ but evolves with $\sigma = 1N/m$ under the same load. Figure 7d shows that the larger interface energy leads to larger damaged area. The effect of kinetic coefficient is shown in Fig. 7e similar to the previous examples.

6 Conclusion

A multi-phase-field approach for fracture is presented. The model is applicable but not limited to the polycrystalline materials where there are solid-solid interfaces between the grains or phases.
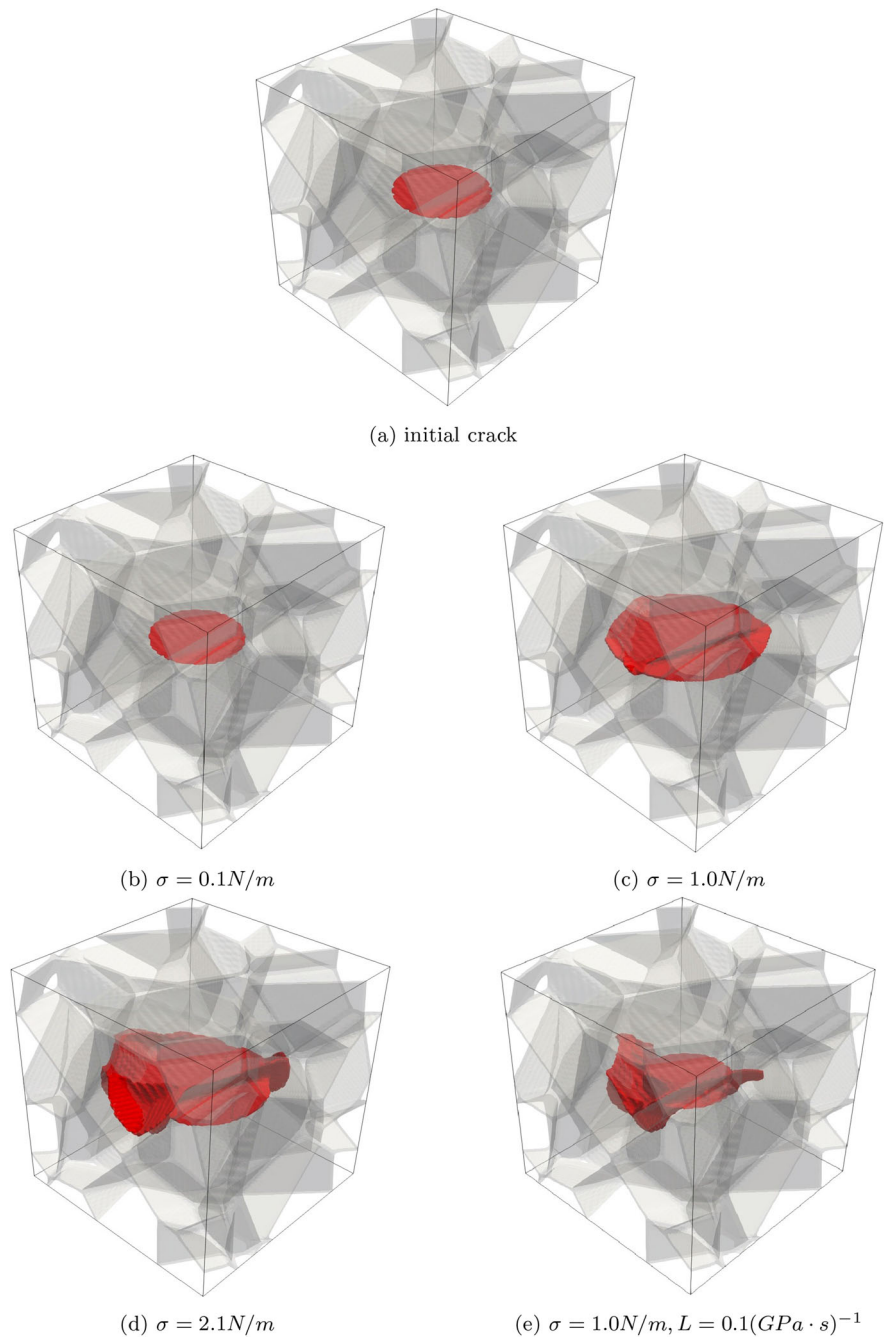
The model has the following novel features:

Fig. 6 Fracture phase-field for different value of grain boundary σ energy and kinetic coefficient L

(a) initial crack

(b) $\sigma = 0.1 N/m$

(c) $\sigma = 1.0 N/m$

(d) $\sigma = 2.1 N/m$

(e) $\sigma = 1.0 N/m, L = 0.1 (GPa \cdot s)^{-1}$

(1) The interface energy is included from the very beginning into the model description. The free energy includes one additional term for the interface energy which degrades in the crack region.

(2) The contribution of the interface energy is explicitly taken into Ginzburg-Landau equation for fracture.

Thus, the elastic energy release rate is not the only driving force for fracture but the relaxation of interface energy during damage evolution also drives the crack. The results can also be interpreted in terms of the classical fracture mechanics, $G^e > \Delta G$, where G^e is the elastic energy release. There are

(a) initial crack

(b) $\sigma = 0.1 N/m$

(c) $\sigma = 1.0 N/m$

(d) $\sigma = 2.1 N/m$

(e) $\sigma = 1.0 N/m, L = 0.1 (GPa \cdot s)^{-1}$

two options for the change in surface energy of the crack, ΔG: for crack propagating through the bulk $\Delta G = G$ and for crack propagating through the interfaces $\Delta G = G - \sigma$. This means that in the current model the elastic energy threshold for fracture is lower if the interface energy relaxes during damage.

(3) The finite difference method is utilized to solve the complete system of the phase-field and mechanics equations in 2D and 3D for a polycrystalline material. The importance of the interface (grain boundary) energy is analyzed numerically for various model problems. The results show how the intergranular fracture is promoted by the high inter-

face energy, while for low interface energy, crack is mostly controlled by the elastic energy release.

Note that other continuum-based approaches like peridynamics have shown promising results in fracture problems (Mehrmashhadi et al. 2020). Zhang et al. 2018 used peridynamics approach to study a computational polycrystalline structure with the same average grain size as the samples used in experiments. Their peridynamic results helped explain the reasons behind the observed failure front supershear propagation speed, and the subsequent transition to sub-Rayleigh propagating localized cracks. They found that the presence of microstructure can be "protective" against dynamic fracture because material interfaces and anisotropy can slightly disperse waves that cause damage

Declarations

Conflict of interest The authors declare no competing interests.

References

Abdollahi A, Arias I (2012) Numerical simulation of intergranular and transgranular crack propagation in ferroelectric polycrystals. Int J Fract 174:3–15

Amiri F, Millán D, Arroyo M, Silani M, Rabczuk T (2016) Fourth order phase-field model for local max-ent approximants applied to crack propagation. Comput Methods in Appl Mech Eng 312:254–275. https://doi.org/10.1016/j.cma.2016.02.011

Amirian B, Jafarzadeh H, Abali BE, Reali A, Hogan JD (2022) Phase-field approach to evolution and interaction of twins in single crystal magnesium. Comput Mech 70:803–818

Amirian B, Jafarzadeh H, Abali BE, Reali A, Hogan JD (2022) Thermodynamically-consistent derivation and computation of twinning and fracture in brittle materials by means of phase-field approaches in the finite element method. Int J Solids Struct 252:111789

Benjamin E. Grossman-Ponemon, Ataollah Mesgarnejad, Alain Karma, Phase-field modeling of continuous fatigue via toughness degradation, Engineering Fracture Mechanics, Volume 264, 2022, 108255

Clayton JD, Knap J (2011) A phase field model of deformation twinning: nonlinear theory and numerical simulations. Physica D 240:841–858

Clayton JD, Knap J (2014) A geometrically nonlinear phase field theory of brittle fracture. Int J Fract 189:139–148

Fantoni F, Bacigalupo A, Paggi M, Reinoso J (2020) A phase field approach for damage propagation in periodic microstructured materials. Int J Fract 223:53–76

Farrahi GH, Javanbakht M, Jafarzadeh H (2020) On the phase field modeling of crack growth and analytical treatment on the parameters. Continuum Mech Thermodyn 32:589–606

Francfort GA, Marigo J-J (1998) Revisiting brittle fracture as an energy minimization problem. J Mech Phys Solids 46(8):1319–1342

Ghaedi MS, Javanbakht M (2021) Effect of a thermodynamically consistent interface stress on thermal-induced nanovoid evolution in NiAl. Math Mech Solids 26:1320–1336

Grossman-Ponemon BE, Mesgarnejad A, Karma A (2022) Phase-field modeling of continuous fatigue via toughness degradation. Eng Fract Mech 264:108255

Hansen-Dörr AC, de Borst R, Hennig P, Kästner M (2019) Phase-field modelling of interface failure in brittle materials. Comput Methods Appl Mech Eng 346:25–42

Hofacker M, Miehe C (2012) Continuum phase field modeling of dynamic fracture: variational principles and staggered FE implementation. Int J Fract 178:113–129

Hossain M, Hsueh C-J, Bourdin B, Bhattacharya K (2014) Effective toughness of heterogeneous media. J Mech Phys Solids 71:15–32

Hu S, Chen L (2001) A phase-field model for evolving microstructures with strong elastic inhomogeneity. Acta Mater 49:1879–1890

Jafarzadeh H, Mansoori H (2020) Phase field approach to mode-I fracture by introducing an eigen strain tensor: general theory. Theoret Appl Fract Mech 108:102628

Jafarzadeh H, Levitas VI, Farrahi GH, Javanbakht M (2019) Phase field approach for nanoscale interactions between crack propagation and phase transformation. Nanoscale 11:22243–22247

Jafarzadeh H, Farrahi GH, Javanbakht M (2020) Phase field modeling of crack growth with double-well potential including surface effects. Continuum Mech Thermodyn 32:913–925

Jafarzadeh H, Farrahi GH, Levitas VI, Javanbakht M (2022) Phase field theory for fracture at large strains including surface stresses. Int J Eng Sci 178:103732

Karma A, Kessler DA, Levine H (2001) Phase-field model of mode III dynamic fracture. Phys Rev Lett 87:45501

Khachaturyan AG (1983) Theory of structural transformations in solids. Wiley, New York

Levitas VI, Javanbakht M (2011) Phase-field approach to martensitic phase transformations: effect of martensite–martensite interface energy. Int J Mater Res 102:652–665

Levitas VI, Javanbakht M (2012) Advanced phase-field approach to dislocation evolution. Phys Rev B 86:140101

Levitas VI, Preston DL (2002) Three-dimensional Landau theory for multivariant stress-induced martensitic phase transformations. I. Austenite ↔ martensite. Phys Rev B 66:134206

Levitas VI, Jafarzadeh H, Farrahi GH, Javanbakht M (2018) Thermodynamically consistent and scale-dependent phase field approach for crack propagation allowing for surface stresses. Int J Plast 111:1–35

Mehrmashhadi J, Bahadori M, Bobaru F (2020) On validating peridynamic models and a phase-field model for dynamic brittle fracture in glass. Eng Fract Mech 240:107355

Mesgarnejad A, Imanian A, Karma A (2019) Phase-field models for fatigue crack growth. Theor Appl Fract Mech 103:102282

Msekh MA, Silani M, Jamshidian M, Areias P, Zhuang X, Zi G, He P, Rabczuk T (2016) Predictions of J integral and tensile strength of clay/epoxy nanocomposites material using phase field model. Compos Part B: Eng 93:97–114. https://doi.org/10.1016/j.compositesb.2016.02.022

Nestler B, Garcke H, Stinner B (2005) Multicomponent alloy solidification: phase-field modeling and simulations. Phys Rev E 71(4):041609

OpenPhase–phase-field simulation software library, www.openphase.rub.de

Oshima K, Takaki T, Muramatsu M (2014) Development of multiphase-field crack model for crack propagation in polycrystal. Int J Comput Mater Sci Eng 03(02):1450009

Rahbar H, Javanbakht M, Ziaei-Rad S, Reali A, Jafarzadeh H (2022) Finite element analysis of coupled phase-field and thermoelasticity equations at large strains for martensitic phase transformations based on implicit and explicit time discretization schemes. Mech Adv Mater Struct 29(17):2531–2547

Schneider D, Schoof E, Huang Y, Selzer M, Nestler B (2016) Phase-field modeling of crack propagation in multiphase systems. Comput Methods Appl Mech Eng 312:186–195

Schöller L, Schneider D, Herrmann C, Prahs A, Nestler B (2022) Phase-field modeling of crack propagation in heterogeneous materials with multiple crack order parameters. Comput Methods Appl Mech Eng 395:114965

Shchyglo O, Guanxing D, Engels JK, Steinbach I (2019) Phase-field simulation of martensite microstructure in low-carbon steel. Acta Mater 175:415–425

Spatschek R, Müller-Gugenberger C, Brener E, Nestler B (2007) Phase field modeling of fracture and stress-induced phase transitions. Phys Rev E 75:066111

Steinbach I (2009) Phase-field models in materials science. Modell Simul Mater Sci Eng 17:073001

Steinbach I, Pezzolla F (1999) A generalized field method for multiphase transformations using interface fields. Physica D 134(4):385–393

Yin B, Zhao D, Storm J, Kaliske M (2022) Phase-field fracture incorporating cohesive adhesion failure mechanisms within the representative crack element framework. Comput Methods Appl Mech Eng 392:114664

Zhang G, Gazonas GA, Bobaru F (2018) Supershear damage propagation and sub-Rayleigh crack growth from edge-on impact: a peridynamic analysis. Int J Impact Eng 113:73–87